Chapter 5

Implications for Geology

The sources of the continental magnetic anomalies primarily consist of rock types formed early in the geological history of the earth. A glance at the observed magnetic anomaly map and the geological map of the world clearly points to the fact that most of the anomalies lie over the geological regions Precambrian in age. However, the exposed Precambrian rocks constitute only 29% of the total Precambrian crust (Goodwin, 1991). This means that a significant portion of the oldest crust on Earth is overlain by Phanerozoic cover. Hence, our aim is to look for the possible extensions of the Precambrian units obscured by younger cover and add to the existing information on geological boundaries of the Precambrian units. For this purpose, it is necessary to first consider the known geology of the region and its boundaries at the surface. Subsequently, using our modelling procedure, the vertical field anomaly map is computed for the region and compared with the corresponding region of the CHAMP magnetic anomaly map. The next step is to modify the boundary of the region and to recompute the anomaly map until a reasonable fit is achieved with the observed anomaly map. The modelling results are presented for some of the provinces of the world that have a distinct magnetic signature but are largely buried under Phanerozoic cover. The provinces (1-6) considered for detailed analysis are shown in the World geological map (CGMW, 2000) (Fig. 5.1a) and in *initial model* vertical field magnetic anomaly map (Fig. 5.1b) as white rectangles.

These six regions are chosen due to the particular tectonic settings, which causes these anomalies. The anomaly at Kentucky-Tennessee region(1), North America, is due to mid Proterozoic anorogenic magmatic activity. The granite and anorthosite massifs so abundant in this province are produced by partial melting of the lower crust. Thus, it would be interesting to map the areal extent of this magmatic activity as the region is largely buried under Phanerozoic cover. The next region of our study is Greenland(2). Largely buried under ice, without much information about its central region, it would be interesting to infer the rock types based on the observed magnetic anomaly map. The next region for our investigation is west and central Africa. The investigation of the thickness of magnetic crust below the West African craton(3) is carried out. In central Africa, over the Bangui region(4), there is disagreement between the predicted and observed magnetic anomaly map. By further study, the composition of lower crust is inferred from the intensity of the observed magnetic anomaly pattern in the region. Geological units in the eastern region of Siberia comprises mostly of accreted regions (Fujita, 1978, Churkin and Trexler, 1980), including the Kolyma and Omolon blocks(5). During the early Jurassic,

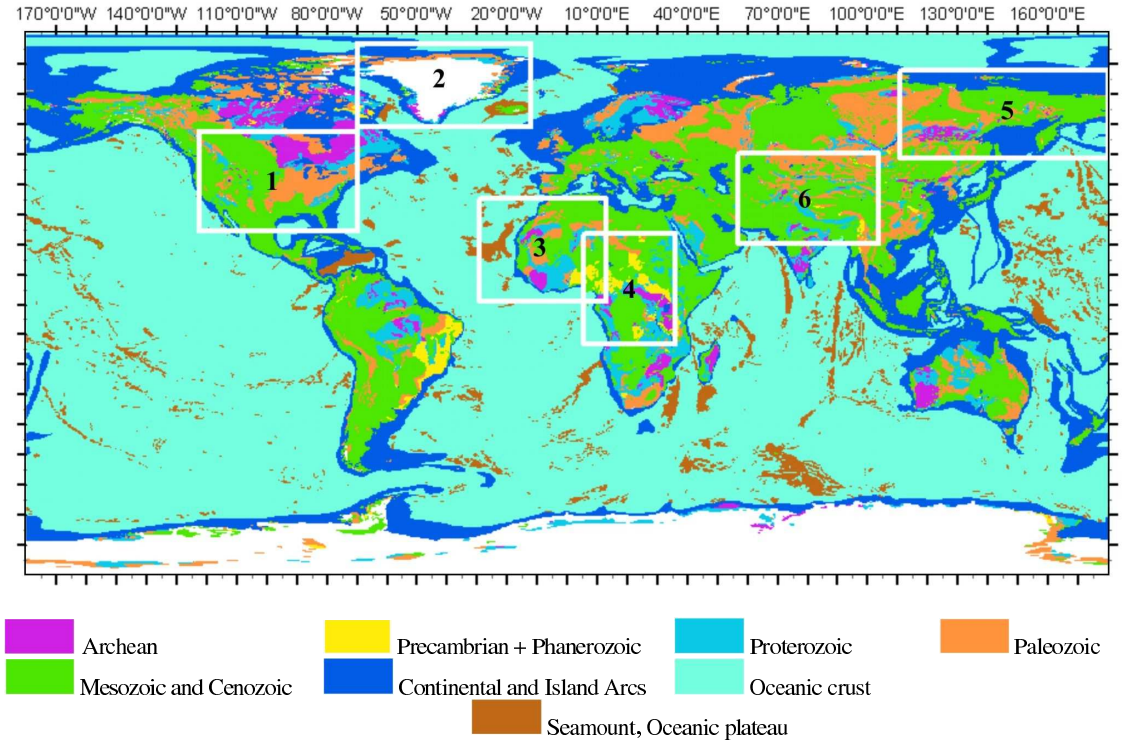

Fig. 5.1a. World geological map (CGMW, 2000). The white rectangles show the areas to be studied in this chapter.

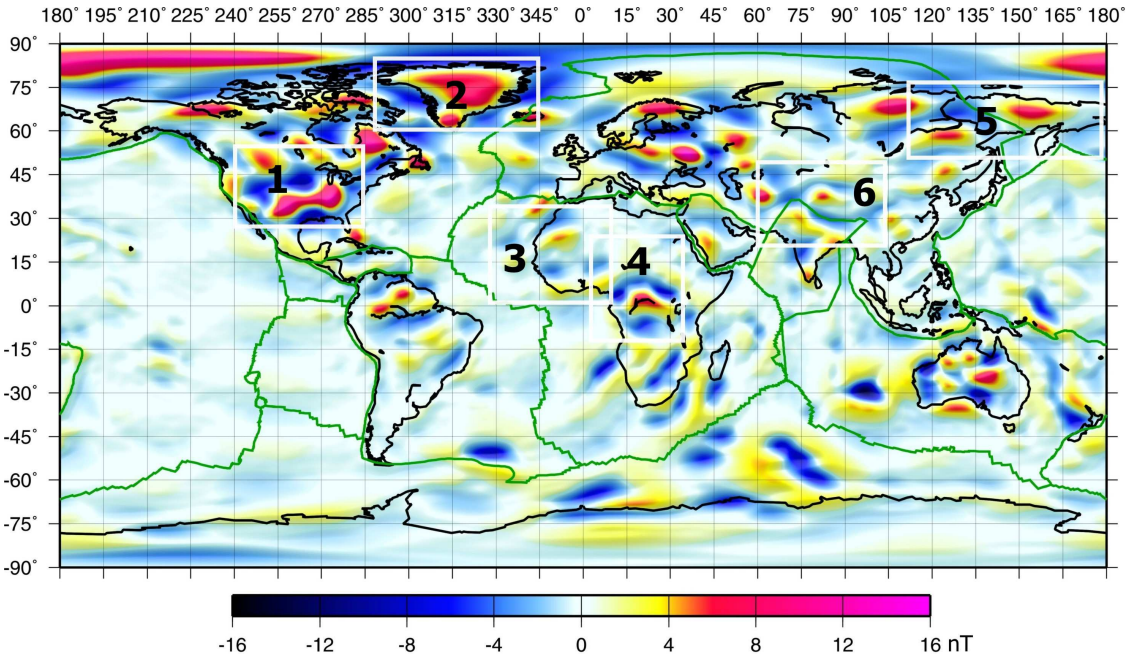

Fig 5.1b. *Initial model* vertical field anomaly map for spherical harmonic degrees 16-80 at an altitude of 400 km shown in cylindrical equidistant projection.

Chukotsk block collided with East Siberia, deforming both these blocks and caused the formation of Cherskiy suture zone. The deformation of the Kolyma block in particular,

during the continent-continent type collision that lasted till early Tertiary is investigated in detail here. Finally, the extension of basement of a rigid block on the Cathaysian plate, the Tarim craton(6), is studied. At the center of the craton lie the Archean rocks, and rocks of early and late Proterozoic ages surround them. Here, I investigate in detail, whether the Archean rocks extend below these Proterozoic rocks or not.

5.1 Kentucky-Tennessee region, North America

Central Province (Belt) is a large structural province, which underlies the south-central USA, occupying the southern portion of the North American craton. The rocks of this province are exposed only in a few places in Colorado and California. Large anorogenic magmatic activity is dominant along the entire stretch of this province (Goodwin, 1991). Figure (5.2) shows the tectonic boundary of this province as envisaged by Anderson (1983), inferred from anorogenic granite intrusions in the upper crust. The granites and associated anorthosites in this province are of two ages, flanking the eastern and the western halves. Major subprovinces of 1.34-1.40 Ga and 1.42-1.50 Ga granites occur in these two halves (Fig. 5.2). Geochemically, these anorogenic granites are A-type granites enriched in K and Fe and depleted in Ca, Mg and Sr. This means A-type granites are more magnetic relative to I- and S-type granitic bodies (Ishihara, 1977; 1987). The composition of granites suggest an origin in the lower crust (25-35 km) and are produced by partial melting of lower crustal rocks of intermediate or mafic composition (Condie, 1978).

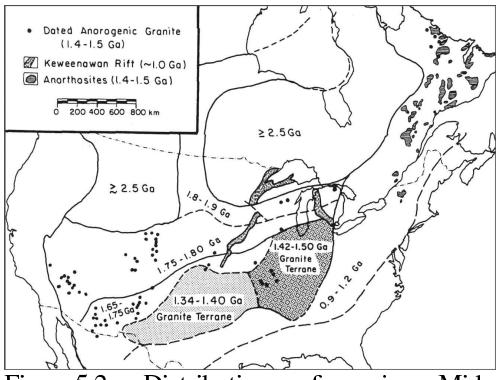

Fig. 5.2. Distribution of major Mid-Proterozoic anorogenic granites and anorthosites in North America. (Anderson, 1983).

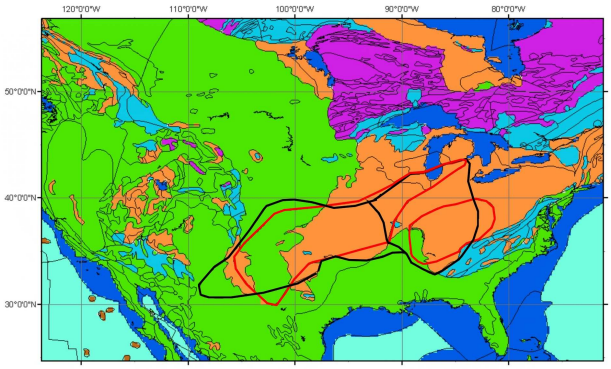

Fig. 5.3. The geological map of the southwest USA region. Thick black line is the previous boundary and the red line marks the new boundary.

The presumed present extent of the boundary (Anderson, 1983) of this buried mid-Proterozoic province is taken as input to the GIS based model. The modelling steps are described in chapter 2, where the initial VIS model is derived. The initial vertical field over the mid-Proterozoic province, southwest USA (Fig. 5.1b), shows an apparent mismatch in the extent of the predicted anomaly as compared to the observed anomaly pattern in Figure (5.4b). The predicted anomaly over the southwestern region of the province extend beyond the boundary defined by the observed map. Over the eastern region of the mid-Proterozoic province, the predicted anomaly extends up to the base of Lake Michigan. This differs significantly from the observed map, which shows an oval-

shaped positive anomaly only over the Kentucky-Tennessee region. Obviously, the extension of the mid-Proterozoic anorogenic region needs to be redefined.

Figure (5.4a) shows the predicted vertical field anomaly after the boundary of the granitic intrusion was refined in the location where it is most intense and occupies almost the entire crust. This refined model is called *first iteration* model. The redefined boundary is marked with a red line in the geological map of the southwest USA (Fig 5.3). The observed (Fig. 5.4b) and the *first iteration* model are now in better agreement. The oval at the Kentucky-Tennessee region is reproduced accurately. The anomaly pattern over the southwest of the province agrees well. The extension of the predicted anomaly in the northeast direction following up to the base of the Lake Michigan, however, is only partially reproduced. The *first iteration* model results indicate that the granitic intrusion may not occupy the entire crustal column especially in the western flank of the anomaly pattern. In the region between (-90^0)-(-100^0) of the mid-Proterozoic province, the granitic intrusion does not fill the lower 2.0 km of the crustal section while in the region west of -100^0 longitude unoccupied thickness of the intrusion is 5.0 km. Thus the thickness of intruded granites becomes thinner towards the west of the anomaly pattern. Recent results from Purucker et al. (2002) for the North American craton using the a priori model comprising both induced and remanent magnetisation as the source also showed good agreement with the observed anomaly map derived using the Ørsted satellite data. They concluded that remanence may not be important for modelling the continental anomalies and that induced magnetisation can explain the observed magnetic anomaly patterns.

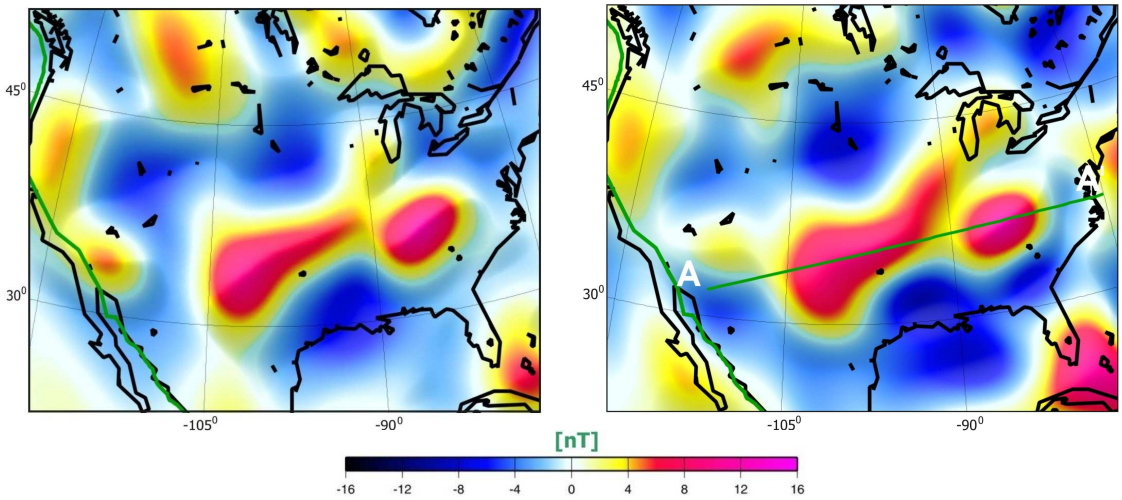

Fig. 5.4a. *First iteration* (predicted) vertical field anomaly map for spherical harmonic degrees 16-80 at an altitude of 400 km following the boundary of mid-Proterozoic province shown in Fig.5.2.

Fig. 5.4b. Observed vertical field anomaly map for spherical harmonic degrees 16-80 at an altitude of 400 km for the southwest USA region. Line AA' show the profile section.

Figure (5.5) shows the profile along the marked section AA' extracted from the observed map, and from the *initial model* and *first iteration* predictions. The profile allow for a better comparison of the amplitude of the anomalies.

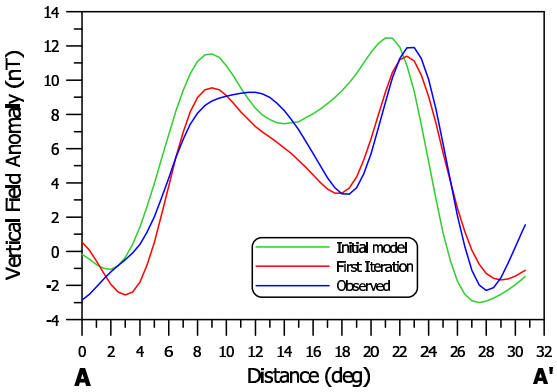

Fig. 5.5. Profile section along AA', shown for *initial model* (green line), *first iteration* (red line), and the observed anomaly (blue line) map.

5.2 North-Greenland, Greenland

The observed vertical field anomaly map of northern Greenland (Fig. 5.8b) clearly shows a disagreement with the *initial model* map for the same region (5.1b). A large anomaly predicted for the central portion of Greenland is not present in the observed map. The observations show a linear trend in the E-W direction across the center of northern Greenland. This discrepancy cannot be resolved easily because more than 90% of Greenland is under a cover of thick ice, obscuring the geology beneath it. Nevertheless, some recent geophysical studies over central Greenland have provided new insights into the nature of the crust below the ice cover. Our efforts here would be to use some of these results to improve our *initial model* and possibly try to explain a possible geological situation that could be a source of the anomaly observed.

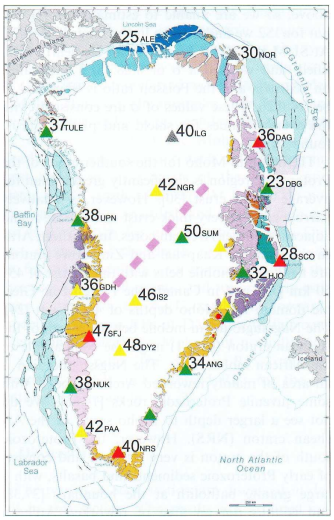

Fig. 5.6. Depths to Moho in km for all the stations in the map of Greenland. The suggested division of the Proterozoic part of Greenland is marked in pink (Dahl-Jensen, 2003).

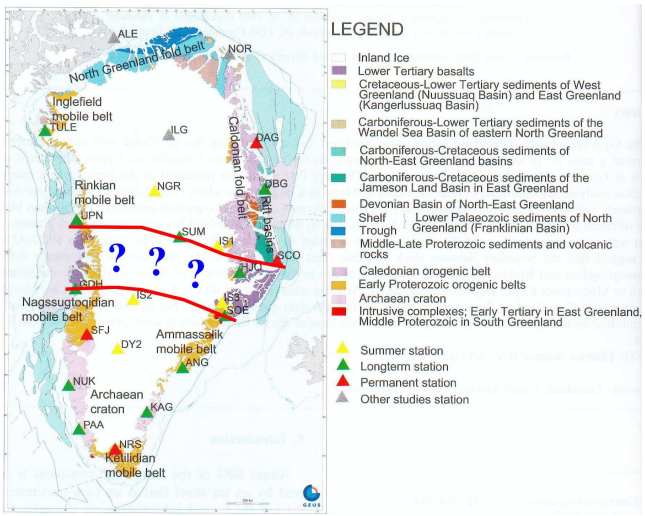

Fig. 5.7. Geological map of Greenland (Henriksen, 2000). The region marked in red line is the possible plume passage and symbol '?' suggests that it has not been proved (Wölbern et al., 2001).

The recent seismic results of Dahl-Jensen (2003), show the crustal thickness variations for entire Greenland (Fig. 5.6). However, the more interesting information that came out of their work is the delineation of the boundary that separates the northern and southern Greenland blocks of different Proterozoic ages. This boundary separating these northern and southern blocks runs from the western flank of Naggastoquidian belt in a northeast direction and terminates before reaching the eastern coast of Greenland (Fig. 5.6). The numbers in Figure (5.6) are depths to Moho at various stations across Greenland. The geological map of Greenland (Henriksen, 2000) is shown in Figure (5.7). Taking this new seismic model and assuming the block south of this boundary to have a lower susceptibility (0.0204 SI) than the upper block (0.0404 SI), the *initial model* is modified. The resulting *first iteration* VIS model predicts the vertical field anomaly map shown in Figure (5.8a) and is to be compared with the observed vertical field magnetic map (Fig. 5.8b).

The resulting *first iteration* model shows a better-constrained anomaly pattern over north Greenland. The elongated anomaly feature trending east-west in the observed map, however, is only partially reproduced in the predicted map. The amplitudes of the anomaly for *initial model*, *first iteration* model and the observed map along the profile sections AA' and BB' are shown in the Figure (5.9). The amplitude of the *first iteration* anomaly exceeds the amplitude of the observed anomaly amplitude by 1-2 nT. The *first iteration* model for Greenland shows that there may exist a boundary separating the two blocks having different composition. Due to unavailability of rock samples from the central region of Greenland, the study of rocks exposed at both the eastern and western coast of central Greenland could provide a clue.

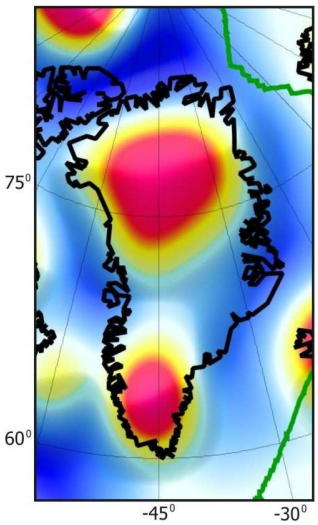

Fig. 5.8a. *First iteration* (predicted) vertical field anomaly map for spherical harmonic degrees 16-80 at an altitude of 400 km for Greenland.

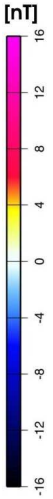

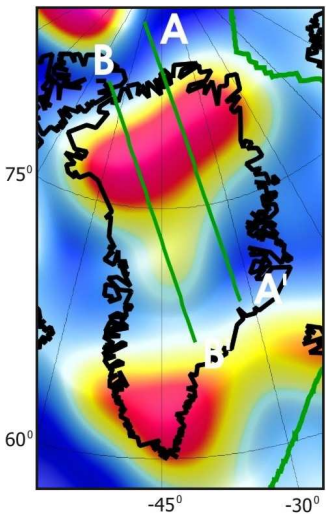

Fig. 5.8b. Observed vertical field anomaly map for spherical harmonic degrees 16-80 at an altitude of 400 km for Greenland. Lines AA' and BB' show the profile sections.

Wölbern et al. (2001) conducted such a study to investigate a possible passage of the Iceland plume below central Greenland. It is known that extensive flood basalts occupy both the eastern and western coast of central Greenland. The flood basalts are generally

an outpouring after the passage of a plume beneath a geological region. Wölbern et al. (2001), through receiver function analysis, however, could not find a signature related to a plume in '410 discontinuity' but could see some signatures at '660 discontinuity'. The work did not quite prove the existence of a plume passage in the geological past. However, assuming that such a phenomenon might have happened, the modelling work of Arkani-Hamed and Strangway (1985b) showed that, a heat source like a plume could cause a demagnetisation of the lower crust. This could be a possibility in central Greenland. The consequence being that the Proterozoic block south of the boundary would be less magnetic than the northern block. Indeed, such a geological setup, as has been modeled above, shows a significant improvement in predicting the anomaly over the region.

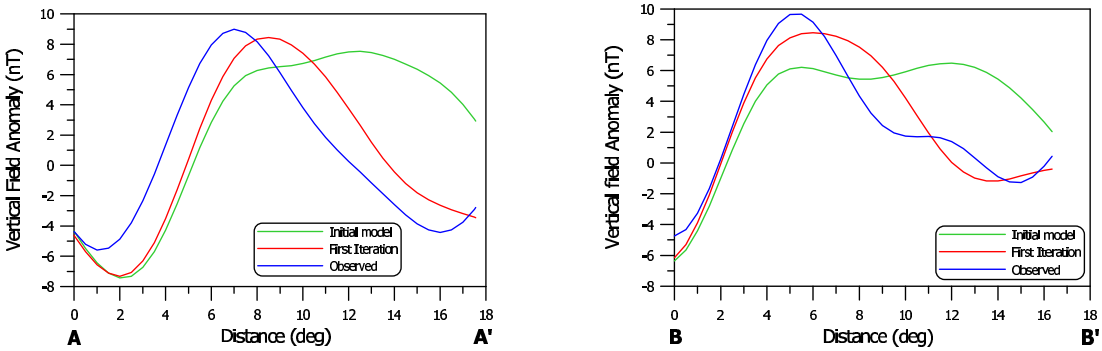

Fig. 5.9. Profile sections along AA' and BB', shown for *initial model* (green line), *First iteration* (red line), and the observed anomaly (blue line) map.

5.3 West African craton, West Africa

In the African continent, the patterns of the anomalies over the West African craton and the Bangui region are fairly well predicted, but the amplitudes fall short of the observed amplitudes. Detailed investigation is carried out to explain the large observed anomaly over these regions.

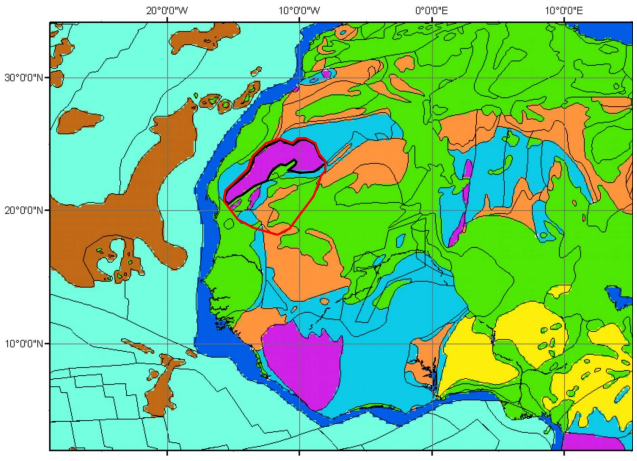

Fig. 5.10. The geological map of the West African region. Thick black line is the previous boundary and the red line marks the new boundary.

Fig. 5.11. The geological map of the West African region (Goodwin, 1991).

In the West African craton, the Archean rocks of Amsaga belts of the Reguibat shield in the north and the Liberian shield in the south, including the exposed Kasila series, is composed of mafic rock constituents (Goodwin, 1991). The VIS value for these regions is shown in Appendix (VI). The observed anomaly map (Fig. 5.12b) shows a band of negative anomaly that extends over the Liberian shield with a strong positive observed over the Kasila series. A positive anomaly of high amplitude is observed over the western Taoudeni basin south of Amsaga Archean belt. The predicted anomaly map (Fig. 5.1b) does reproduce the anomaly pattern; a high over the Taoudeni basin flanked by low anomaly on either side but fails to reproduce the strong amplitude. Even the extension of anomaly over the Taoudeni Basin is not seen in the predicted map.

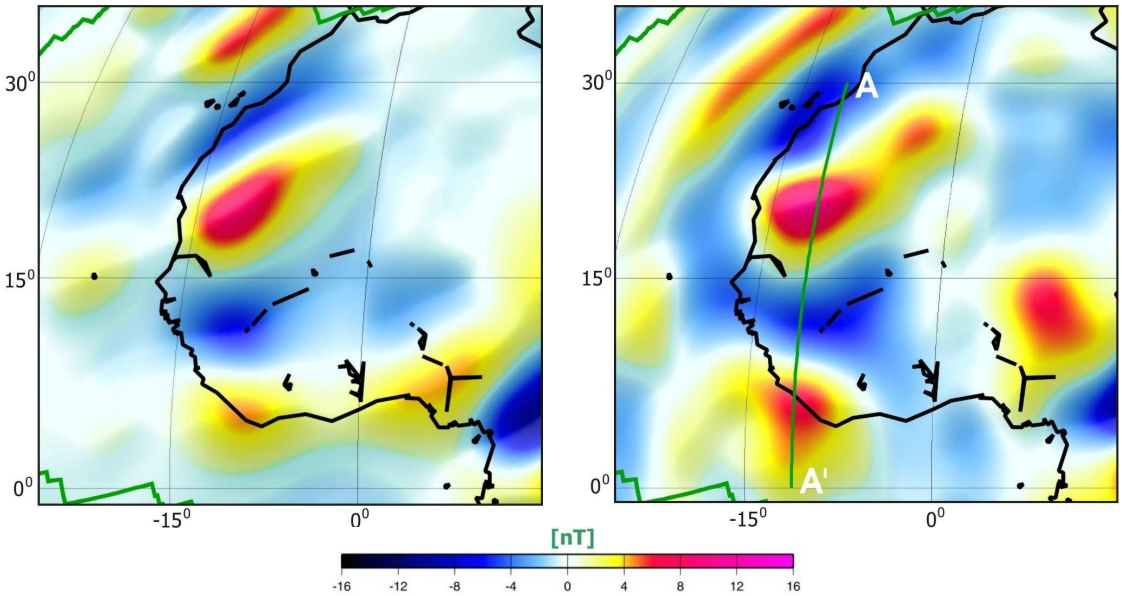

Fig. 5.12a. *First iteration* (predicted) vertical field anomaly map for spherical harmonic degrees 16-80 at an altitude of 400 km for West African region.

Fig. 5.12b. Observed vertical field anomaly map for spherical harmonic degrees 16-80 at an altitude of 400 km for West African region. Line AA' show the profile section.

To account for the missing amplitude, the VIS model is reinvestigated to find the source of the strong observed anomaly. The crustal thickness variation defined by 3SMAC model and used in the *initial model* underestimates the thickness of Archean crust in the West African cratonic region. The 3SMAC thickness of Amsaga Archean belt is 32-35 km and for the Liberian shield is 30-33 km, while the crustal thickness for a typical Archean unit is 40-42 km in most of the regions of the world. In South Africa, it is 35-45 km, (Nguuri, 2001). Toft and Haggerty (1988) even claim that the crust in the south of the West African craton is 70 km thick. The temperature distribution at a depth of 50 km, using heat flow data (Artemieva and Mooney, 2001), also shows that the Curie-isotherm is still deeper in this region. Accounting for the above reported results for the thickness of an Archean crust and for the West African craton in general, the crustal thickness of Amsaga belt and Liberian shield is increased by 8.0 km. The geological map for the West African craton region is shown in Figure (5.10), which shows the new extension of Amsaga belt in red line. Geological units of the West African region are shown in Figure

(5.11). The VIS model is recomputed using the above parameters and the vertical field anomaly map is computed. The *first iteration* map is shown in Figure (5.12a) and the corresponding observed anomaly map in Figure (5.12b). The predicted map shows the anomaly pattern over the West African craton to agree well with the observations. The anomaly over the western Taudeni basin also matches well with the observed anomaly map. The profile across the craton (Fig. 5.13) shows a comparison of the observed anomaly with the initial and *first iteration* model. Amplitude amounting to 1.8-2.4 nT is yet unaccounted for, especially over the shield regions. These results may point to magnetisation extending into the upper mantle, in agreement with results of Toft and Haggerty (1988).

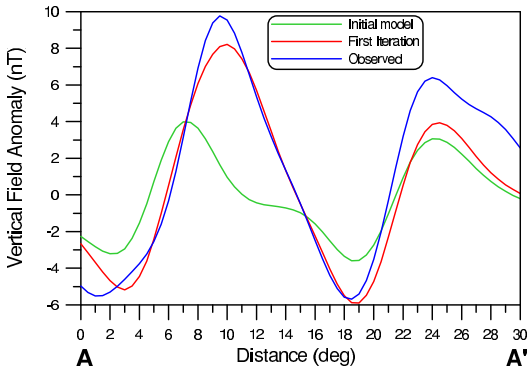

Fig. 5.13 Profile section along AA', shown for *initial model* (green line), *First iteration* (red line), and the Observed anomaly (blue line) map.

5.4 Bangui anomaly, Central Africa

In the Central African region (Fig. 5.14), the region north of Congo craton witnessed Pan-African orogeny (800-530 Ma) that resulted in the intrusion of Oubanguides in the region north of Bangui where it is exposed and along the entire stretch north of Congo craton (Pin and Poidevin, 1987). Figure (5.15) shows the distribution of granulites of the northern part of Congo craton. The high content of iron oxides in two of the three samples showed that they could only be derived from a more mafic parental magma (Clark, 1999). However, the bulk susceptibility of the rock types exposed in the region (Appendix VI) falls short of the total susceptibility required to reproduce the Bangui anomaly. To account for the shortfall in susceptibility, the composition of the lower crust needs to be modified in the model, considering it to be of a more mafic composition than inferred on the basis of surface geology. Emplacement of basalts in the lower crust as a result of Pan-African orogeny is a possibility.

Considering basalts in the lower crust and an additional 4 km of basalts in the upper crust, the computation of VIS in the region north of Congo craton is redone. The vertical field anomaly map is predicted (Fig. 5.16a) and compared with the observed anomaly map (Fig. 5.16b). The *first iteration* magnetic anomaly map for the region now is able to account for most of the missing anomaly. The profile BB' across the anomaly (Fig. 5.17) shows a much better agreement in amplitude with the anomaly in the northern half over Bangui. Over the southern lobe of the anomaly pattern some part of anomaly is yet unaccounted for. This suggests a more mafic composition of the lower crust below Bangui and a more felsic lower crust below Congo craton. A deeper Curie-Isotherm

Fig. 5.14. Geological map of the Central African region (Goodwin, 1991).

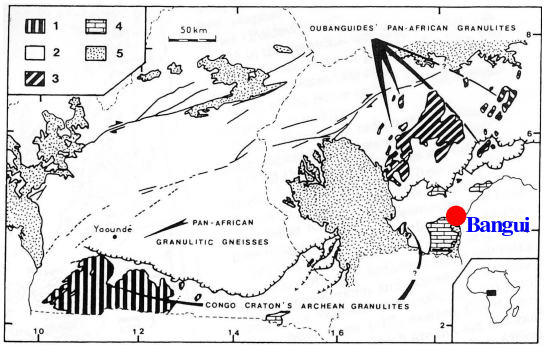

Fig. 5.15. Granulites distribution of the northern part of Congo Craton (Pin and Poidevin, 1987). 1. Archean granulites; 2. Undifferentiated Precambrian formations; 3. Pan-African granulites; 4. Sedimentary upper Precambrian foreland of Oubanguides; 5. Post Pan-African cover.

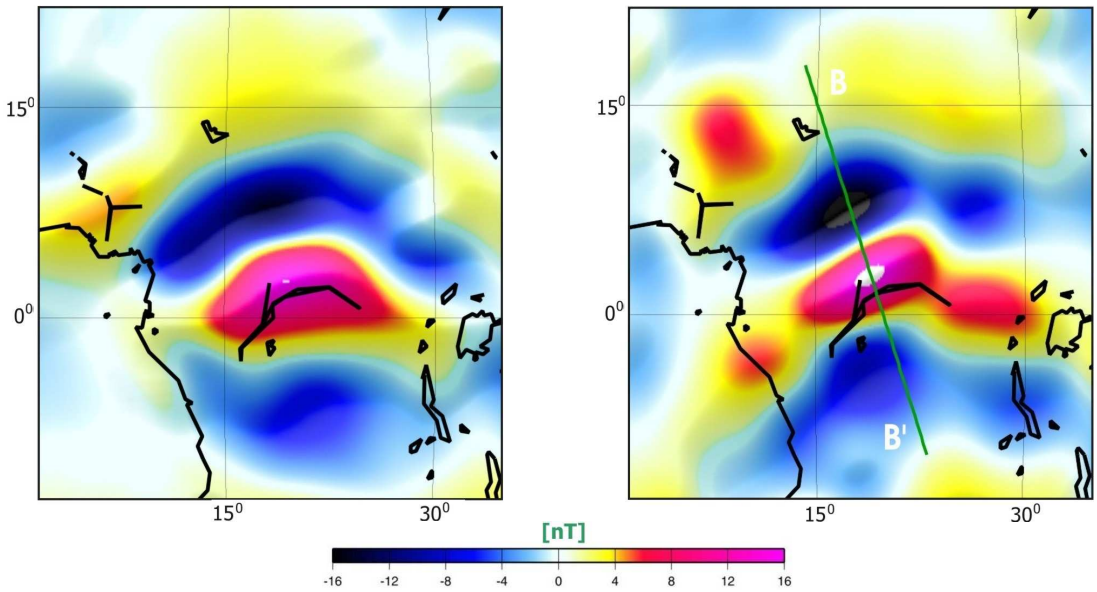

Fig. 5.16a. *First iteration* (predicted) vertical field anomaly map for spherical harmonic degrees 16-80 at an altitude of 400 km for Central African region.

Fig. 5.16b. Observed vertical field anomaly map for spherical harmonic degrees 16-80 at an altitude of 400 km for Central African region. Line BB' show the profile section.

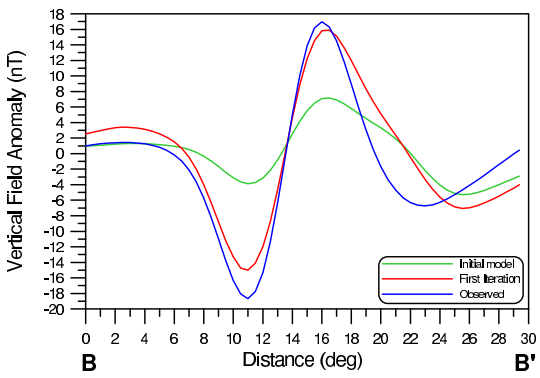

Fig. 5.17 Profile section along BB', shown for *initial model* (green line), *First iteration* (red line), and the observed anomaly (blue line) map.

below Bangui in the northern region and an elevated Curie-Isotherm beneath Congo craton could also possibly account for the missing amplitudes. Indeed, the temperature distribution map at the depth of 50 km prepared by Artemieva and Mooney (2001) supports this argument. Our results are in agreement with Regan and Marsh (1982) who considered the source to be geological and modeled the anomaly by assuming the entire crust below Bangui to be of higher susceptibility (0.01 cgs units) than the surrounding. Ravat et al. (1989) modelled the Bangui anomaly by considering a block of 3.0 km thick of susceptibility 1.0 SI which could be unusually high. The upper crust of the surrounding region was considered felsic while the lower crust was considered more mafic. Girdler et al. (1992) proposed an iron meteorite as the source of the Bangui anomaly.

5.5 Kolyma-Omolon block, Siberia

The region of Kolyma-Omolon block is mostly buried, apart from a few outcrops along the Cherskiy suture zone. The tectonic activity of the region before and after the collision of Brooks-Chukotsk block with East Siberia and West Alaska (Sweeney, 1981; Howell and Wiley, 1987) is shown in Figure (5.18a-d). The shape of Kolyma microcontinent during the early Jurassic period is shown in Figure (5.18a), which surprisingly, until early

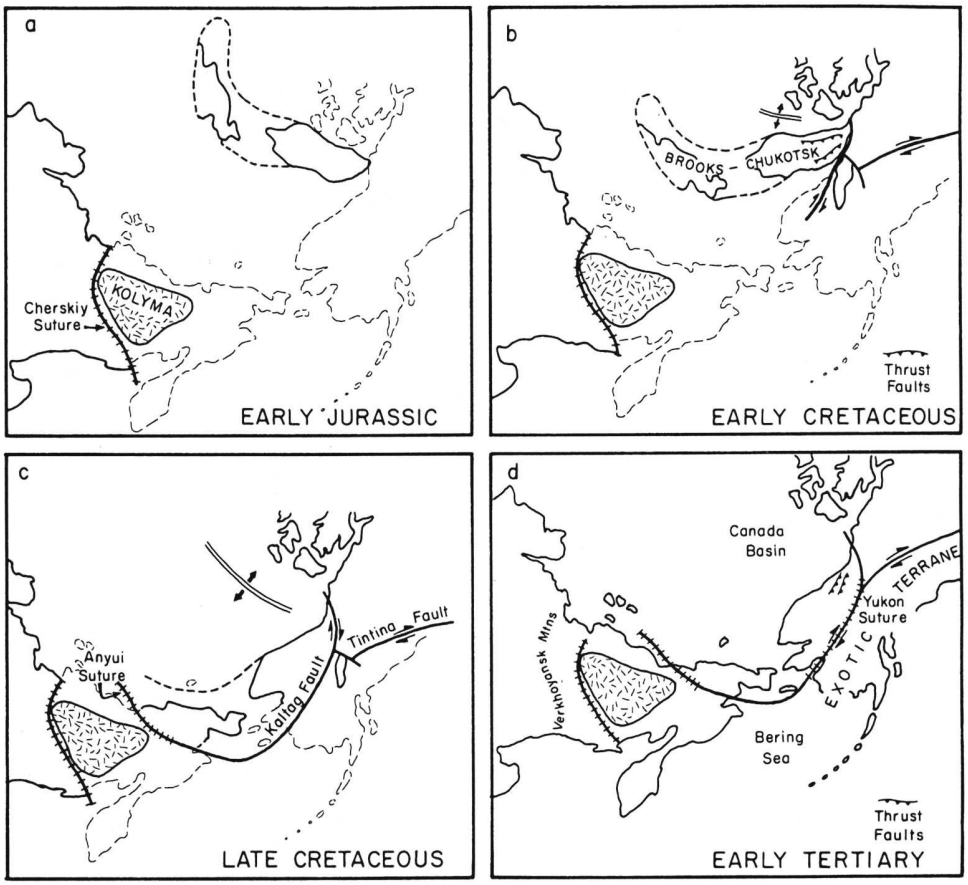

Fig. 5.18. Tectonic reconstruction of the Cordilleran Arctic region since the Early Jurassic (Sweeney, 1981, and Howell and Wiley, 1987. Diagram taken from Condie, (1989).

Tertiary (Fig. 5.18d) was assumed by Sweeney (1981) and Howell and Wiley (1987) to have remained the same. The *initial model* used this shape of the Kolyma block and the vertical component anomaly map was computed accordingly. Obviously, the shape of the predicted anomaly (Fig. 5.1b) did not match with the observations (Fig. 5.20b) over the Kolyma block. The observed map clearly showed an anomaly following the Cherskiy zone trending NW-SE in direction and we investigate the cause for such an anomaly pattern.

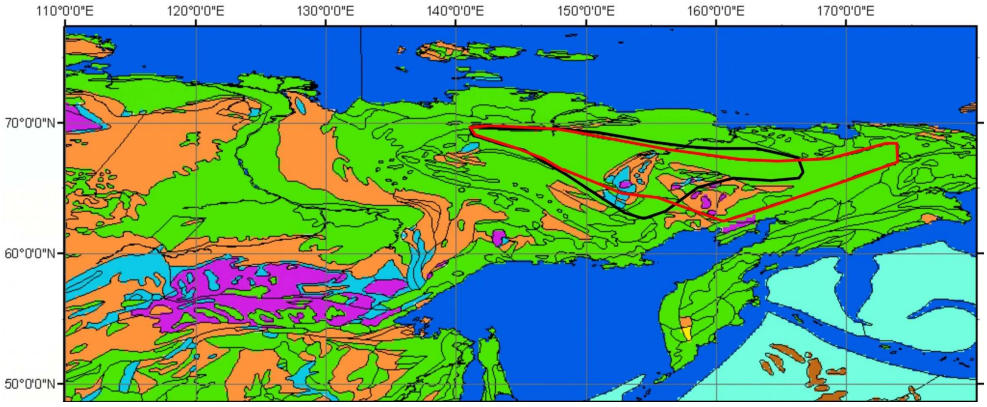

Fig. 5.19. The geological map eastern region of Siberian craton. Thick black line is the previous boundary and the red line marks the new boundary of the Kolyma block.

Keeping in view the intraplate processes that wrenched and internally rotated the Brooks-Chukotsk block on both sides of Bering Sea, it is hard to imagine that the Kolyma block would not have been deformed. Considering that during late-Cretaceous and early Tertiary era, when the Chukotsk block collided with the Kolyma block forming Anyui suture, it compressed the Kolyma block against the Cherskiy Suture zone. This also caused deformation in the Verkhoyansk fold belt located west of Kolyma. The boundary of this deformed Kolyma block, which is hidden under the Phanerozoic cover in the

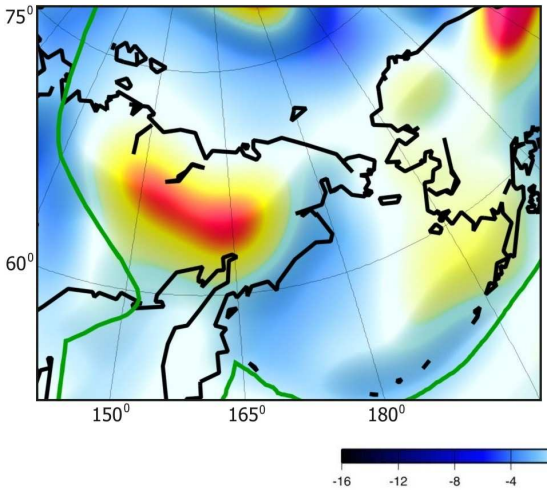

Fig. 5.20a. *First iteration* (predicted) vertical field anomaly map for spherical harmonic degrees 16-80 at an altitude of 400 km for Kolyma block.

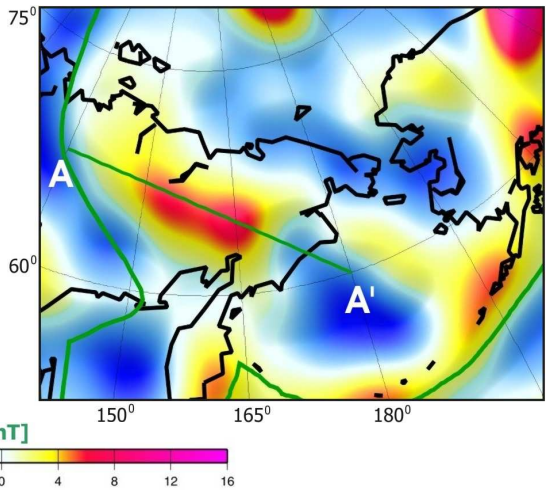

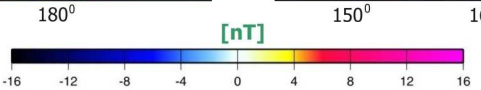

Fig. 5.20b. Observed vertical field anomaly map for spherical harmonic degrees 16-80 at an altitude of 400 km for Kolyma block.

region, is retraced following the observed anomaly pattern over the region. The new boundary is shown in red line in Figure (5.19). The VIS value for the block is recomputed and the vertical field anomaly map for the region is predicted, called the *first iteration* model (Fig. 5.20a). The anomaly associated with the new boundary of the Kolyma block now agree well with the observations (Fig. 5.20b). The profile over the region provides a numerical estimate for the observed and predicted anomaly and is shown in Figure (5.21). Thus, the magnetic anomaly study in this part of the globe demonstrates the ability of the modelling method to trace the subsurface extension of a buried and deformed block.

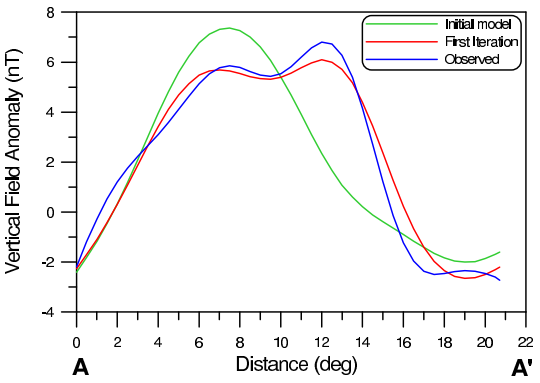

Fig. 5.21. Profile section along AA', shown for *initial model* (green line), *First iteration* (red line), and the observed anomaly (blue line) map.

5.6 Tarim basin, China

Tarim craton or basin is one of the largest rigid blocks, located in the eastern region of the Tibetan plateau. The block is so rigid that it did not get deformed during the Himalayan orogeny. Exhibiting a typical eastward tapered oval shape, and congregation of rock types of different age, a large anomaly over the entire block makes it distinctly different from other blocks of same age. The geology of the region is known only partly, especially with regard to the basement (Zhang et al., 1984) as it is exposed only at the peripheral region of the basin (Fig. 5.22). The exposed Archean rocks occupy the core of the block while a part of the northern region of the block is marked by the presence of early Proterozoic rocks. Mid Proterozoic rocks occupy the rest of the eastern tapered region of the block. Considering all the rock types exposed in the region, including the Phanerozoic sediments covering them, the VIS model is computed for the region. The *initial model* (Fig. 5.1b) predicted for the region is compared with that of the observed magnetic anomaly map (Fig. 4.3a). The anomaly from the predicted map does not match with the observations over the Tarim basin, except only over the core of the block, where the agreement is better.

It is apparent that the susceptibility contrast for the rock types exposed in the surrounding region i.e., of early Proterozoic and mid-Proterozoic is not sufficiently high to produce a strong positive anomaly observable at satellite altitude. The only way this contrast can be generated is to consider the Tarim block entirely comprising of Archean basement. Thus in our derivation of *first iteration* VIS model, the entire basement of Tarim basin is considered to be Archean. The renewed VIS model for the block is computed and the vertical field anomaly map for the Tarim basin is predicted. On comparison of the *first iteration* model (Fig. 5.23a) with the observed anomaly map (Fig. 5.23b), the predicted

anomaly over the Tarim basin is now in better agreement with the observations. The profile sections over the Tarim basin (Fig. 5.24) provide a numerical estimate of the amplitudes of the observed and predicted anomaly maps. Thus, through our modelling studies it can be inferred that the Archean rock exposed only at the core actually occupy the entire basement region of Tarim basin.

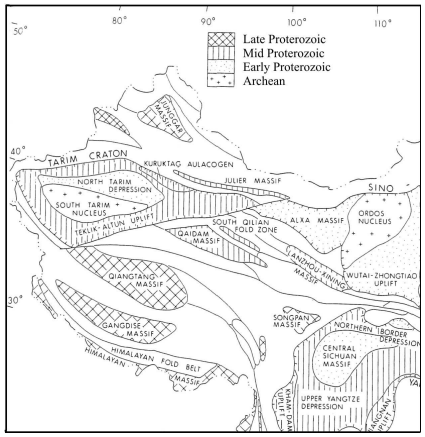

Fig. 5.22. Main outline of Tarim craton within the Cathayian craton. (Goodwin, 1991).

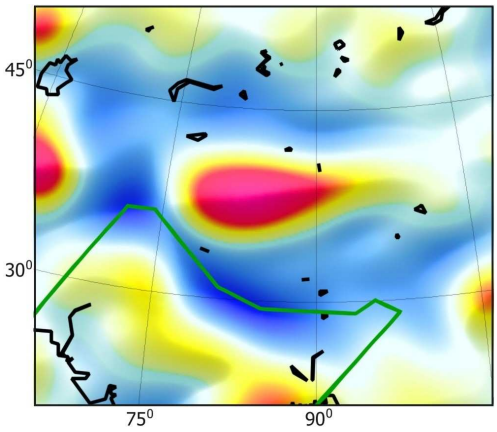

Fig. 5.23a. *First iteration* (predicted) vertical field anomaly map for spherical harmonic degrees 16-80 at an altitude of 400 km for Tarim basin.

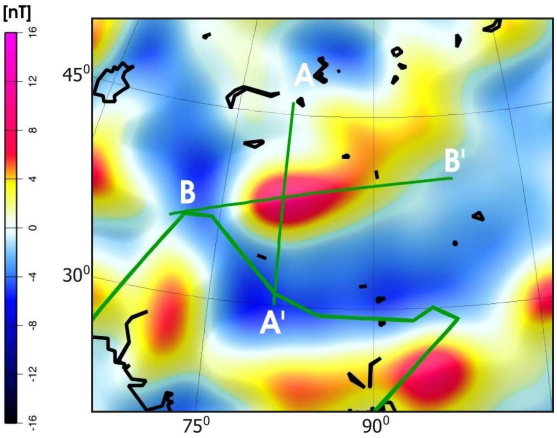

Fig. 5.23b. Observed vertical field anomaly map for spherical harmonic degrees 16-80 at an altitude of 400 km for Tarim basin.

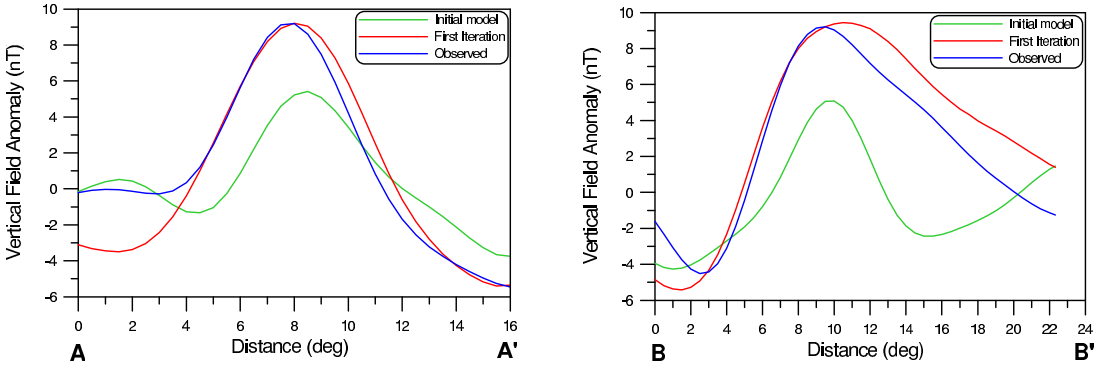

Fig. 5.24. Profile sections along AA' and BB', shown for *initial model* (green line), *first iteration* (red line), and the observed anomaly (blue line) map.

5.7 Global *first iteration* model

In the above sections, we studied the anorogenic magmatic activity and its areal extent, in southwest USA, probable rock types below central Greenland, thickness of crust in West Africa, composition of lower crust in Central Africa, deformation induced to Kolyma block in a continent-continent type collision and finally the extension of Archean basement below Tarim craton. The initial VIS model is modified only in these regions as the predicted anomaly did not match well with the observed anomaly map. Thus, six regions of the world are studied in detail and redefined accordingly and a *first iteration* vertically integrated susceptibility model is derived. Using this *first iteration* VIS model, the *first iteration* vertical field anomaly map is computed at an altitude of 400 km for spherical harmonic degrees 16-80. The VIS model for oceanic region has not been changed since the derivation of initial VIS model. The *first iteration* VIS model and the predicted magnetic anomaly are shown in Figure (5.25) and (5.26) respectively. A detailed comparison has already been done in all the sections above where the anomaly features have improved considerably since the derivation of *initial model*. Here the *first iteration* global magnetic anomaly map is shown for completeness and to have a global view of all the modification done in the above sections.

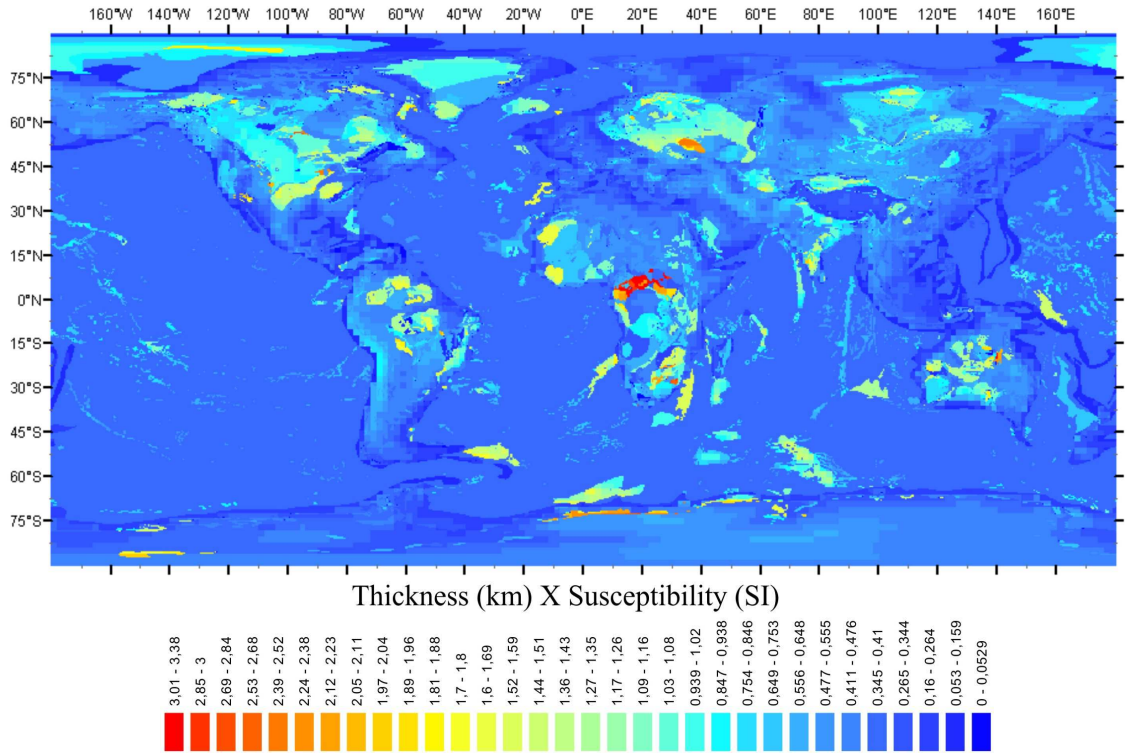

Fig. 5.25. *First iteration* VIS map of the world.

The *first iteration* vertical magnetic anomaly map shown in Figure (5.26) is shown against *initial model* vertical magnetic anomaly map (Fig. 5.27) to compare the improvements achieved after the above exercise.

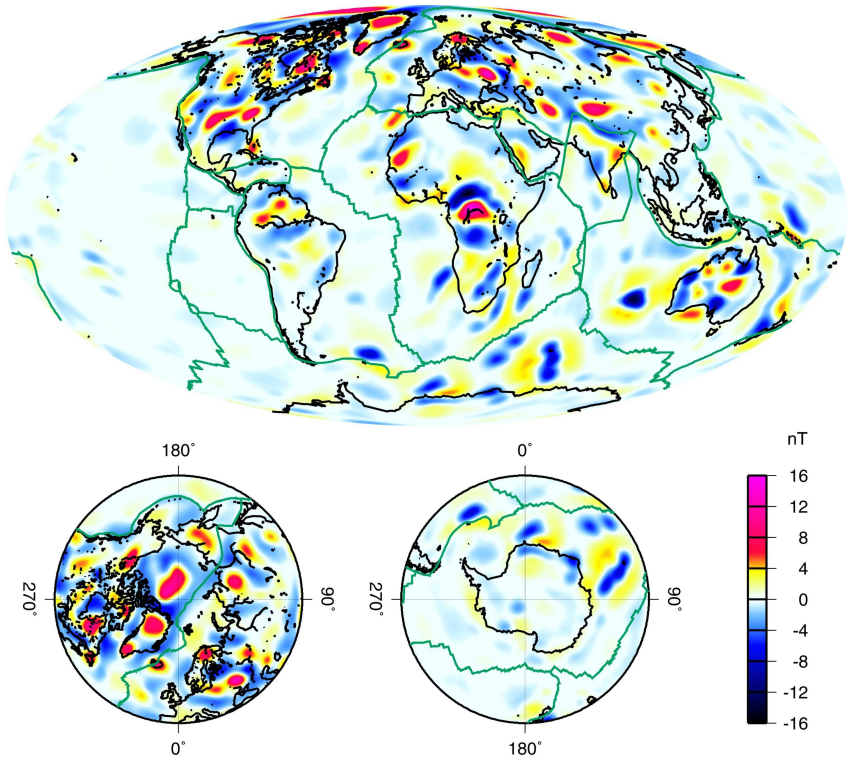

Fig. 5.26. *First iteration* vertical field anomaly map for spherical harmonic degrees 16-80 at an altitude of 400 km.

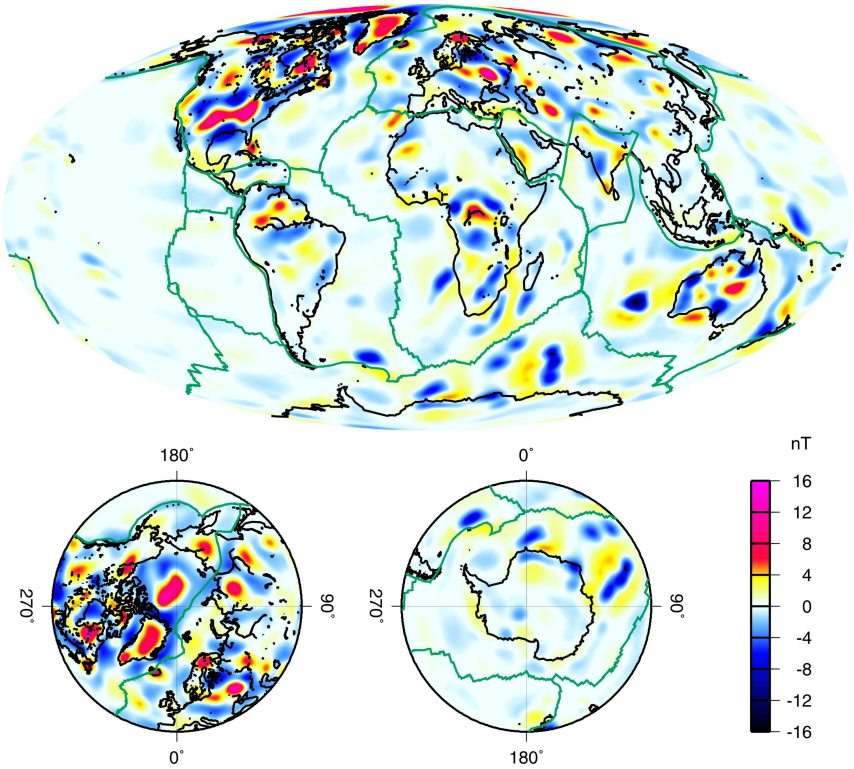

Fig. 5.27. *Initial model* vertical field anomaly map for spherical harmonic degrees 16-80 at an altitude of 400 km.